Defect modification and energy extraction in a one-dimensional terahertz photonic crystal

Sen Liang,[1] Hai-Ying Liu,[1] Qiao-Feng Dai,[1] Li-Jun Wu,[1] Sheng Lan,[1,a)] and Achanta Venu Gopal[2]
[1]*Laboratory of Photonic Information Technology, School for Information and Optoelectronic Science and Engineering, South China Normal University, Guangzhou 510006, People's Republic of China*
[2]*Department of Condensed Matter Physics and Material Science, Tata Institute of Fundamental Research, Homi Bhabha Road, Mumbai 400005, India*

(Received 19 September 2010; accepted 6 December 2010; published online 19 January 2011)

The modification of the defect mode in a one-dimensional (1D) photonic crystal (PC) in terahertz (THz) spectral region was systematically investigated by using THz time-domain spectroscopy (THz-TDS). The 1D PC was constructed by periodically arranging glass slides into an ordered structure. A defect was created by intentionally increasing the separation (i.e., the air gap) between two neighboring glass slides located in the middle of the PC. The tuning of the defect mode in the band gap was demonstrated by changing the thickness of the air gap. Modification of the defect mode was realized by inserting a silicon wafer into the defect. It was found that the appearance of the defect mode in the band gap depends not only on the relative position of the inserted silicon wafer with respect to the beam center but also on the resistivity of the silicon wafer. For the silicon wafer with a high resistivity, a transition of the defect mode from one frequency to the other was observed. When the front end of the silicon wafer was located exactly at the beam center, two defect modes with lower transmittance are observed. For one of the defect modes, the electromagnetic energy stored in the defect can be effectively coupled to the silicon wafer and eventually extracted out of the cavity. When the silicon wafer with a low resistivity was inserted into the defect, only the attenuation of the defect mode was observed. The defect mode disappeared when the beam was completely blocked by the silicon wafer. The large feature size of THz PCs offers us the opportunity of systematically investigating the modification of defect modes in PCs and its applications in the construction of functional devices. The experimental observations obtained by THz-TDS are in good agreement with the numerical simulation results calculated by finite-difference time-domain technique. [doi:10.1063/1.3537824]

I. INTRODUCTION

Photonic crystals (PCs), which are periodic modulation of dielectric constant or refractive index, have been extensively investigated because of their potential applications in the construction of various functional devices in the last two decades.[1,2] In most cases, point defects are intentionally introduced into a PC through modifying the physical properties of certain elements in the PC (e.g., size or refractive index) or breaking the translation symmetry of the PC.[1,2] The defects created in this way can function as cavities or resonators that are important for engineering the spontaneous emission of atoms. On the other hand, PC cavities like this can be employed to construct passive and active optical components such as optical filters,[3] optical delay elements,[4–6] and even optical switches[7–10] and optical limiters[11] when nonlinearity is introduced into the cavities.

In practice, it is highly desirable that the defect mode of a PC cavity can be externally controlled. It means that the field distribution and resonant frequency of the defect mode can be modified by externally altering the physical properties of the defect. A typical example is an optical switch in which the shift in the defect mode or the switching operation is achieved by optically pumping the defect region.[7] For the control of spontaneous emission, an exact match between the resonant frequency of a microcavity and that of a quantum dot (QD) embedded in it is necessary. Since the tuning of the resonant frequency of the microcavity is generally difficult, the match between the two resonant frequencies was usually realized by tuning the resonant frequency of the QD through the change in environmental temperature.[12] In fact, attempt has been made to switch or tune the resonant frequency of a microcavity formed in a PC slab with the tip of an atomic force microscope (AFM).[13] Damping or even disappearance of the defect mode occurred when the tip of the AFM approached the defect region. In addition, a shift in the defect mode was observed when the tip of the AFM was brought into one of the air holes that form the mirrors of the cavity. Physically, it is considered the insertion of the silicon tip would change the effective cavity length and reduce the mirror reflectivity, leading to a shift in the defect mode.[13]

Fabrication and characterization of PCs working in optical wavelength region is not easy because of the small feature size of the constituent elements in PCs. Fortunately, the scaling property of PCs enables the examination and investigation of their physical properties in longer wavelength region [e.g., in microwave or terahertz (THz) spectral region]. The construction of PCs in THz spectral region and the fab-

a)Electronic mail: slan@scnu.edu.cn.

rication of functional devices based on THz PCs have been experimentally investigated and demonstrated.[14,15] The development of THz source, especially ultrashort THz pulses,[16–19] makes it convenient to characterize the transmission properties of various materials and complicated structures with information of both amplitude and phase. Therefore, THz time-domain spectroscopy (THz-TDS) has been widely applied to the characterization of the transmission properties of novel structures, including PCs.[14,15,20–23] Because of the relatively large feature size, PCs in THz spectral region can be easily constructed and they offer us the opportunity to investigate the physical properties of PCs that are not easily accessible in optical wavelength region.

In this paper, we systematically study the modification of the defect mode in a THz PC by gradually inserting a silicon wafer into the defect. A transition of the resonant frequency of the defect mode from one to the other is clearly identified. The coexistence of two defect modes is observed when the front end of the silicon wafer was positioned at the center of the THz beam. In this case, the energy stored in the defect can be partially extracted by the silicon wafer. It is also demonstrated that the modification of the defect mode exhibits a strong dependence on the resistivity of the silicon wafer.

The article is organized as follows. In Sec. II, we describe the fabrication of PCs in THz spectral region and the experimental setup used to implement THz-TDS. Then, the measurement of the complex refractive index of BK7 glass used to construct the PCs by using THz-TDS is presented in Sec. III. In Sec. IV, the transmission spectra for PCs without and with a defect characterized by THz-TDS are examined. The modification of the defect mode by using a silicon wafer is described in Sec. V for a high-resistivity wafer and in Sec. VI for a low-resistivity one. A summary of our research work is given in the conclusion.

II. SAMPLE FABRICATION AND EXPERIMENTAL SETUP

As mentioned above, PCs in THz spectral region are easily fabricated because of their large feature size. In this study, we chose conventional glass cover slides made of BK7 glass to construct the PCs because of three reasons. First, the absorption of BK7 glass is quite small in THz spectral region. Second, its refractive index is much larger in THz spectral region than that in optical wavelength region. This feature makes it possible to fabricate PCs with wider and deeper photonic band gaps (PBGs). Finally, the dispersion of BK7 glass in THz spectral region is negligible.

The PCs used in our study were composed of 170 μm glass slides and 50 μm air gaps. They were fabricated by stacking glass slides one by one with a 50 μm-thick plastic film in between the two neighboring glass slides. Once the glass slides were fixed by curing agent at the edges, all the plastic films were removed, leaving 50 μm air gaps in between the two neighboring glass slides. With these structure parameters, the first PBG of the PC is located at the peak frequency of the THz source which is about 0.30 THz.

In experiments, the one-dimensional (1D) PCs with defects were created by combining two stacks with the same total number of glass slides (four slides for each). One of the stacks (denoted as PC1) was mounted on a diaphragm and the other (denoted as PC2) was fixed onto a three-dimensional (3D) microdisplacement stage. In this way, the air gap between the two stacks, which forms a defect in most cases, can be easily adjusted by the 3D microdisplacement stage. It implies that we can easily control the size of the defect.

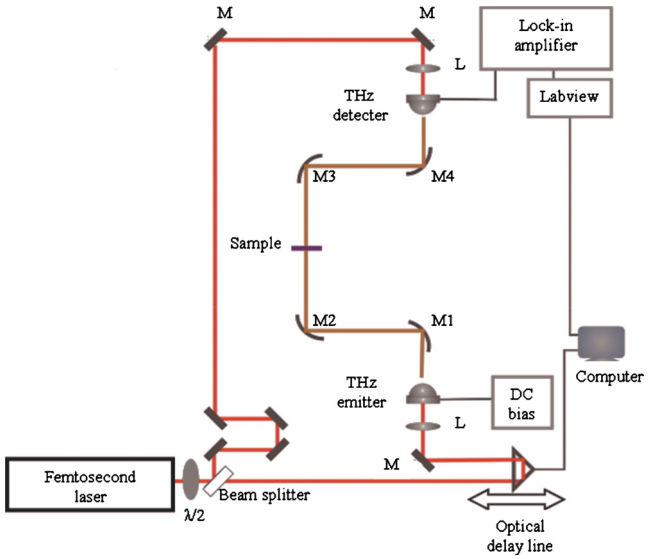

FIG. 1. (Color online) Experimental setup for THz-TDS.

The experimental setup for THz-TDS is schematically depicted in Fig. 1. The 800 nm laser pulses (130 fs and 76 MHz) from a Ti: sapphire oscillator (Mira 900, Coherent) pumped with a solid-state laser (Verdi-5, Coherent) are split into two beams by a beam splitter. One beam is used to excite the photoconductor antenna of the THz emitter (Expla Co.) and the other is used to trigger the THz detector (Expla Co.). The generated THz beam is collimated and focused by four parabolic mirrors arranged in 8-F confocal geometry, providing effective beam coupling between the emitter and the detector. The focus length of the identical inner parabolic mirrors M2 and M3 is 50 mm. The THz beam is focused to a frequency-independent beam with a waist of 3.5 mm in between M2 and M3 where the sample is located. The output signal from the detector is fed into a lock-in amplifier (SR830, Stanford Research Systems) whose output is recorded by a LABVIEW-based data acquisition system. We performed THz-TDS experiments directly in air instead of in a plastic box filled with nitrogen because of two reasons. First, the first PBG of the 1D PC is designed at the peak frequency of the THz source (~0.30 THz) which is below the first absorption peak of water vapor. Second, the tuning of the defect and the insertion of silicon wafer become easier without the use of the box.

III. COMPLEX REFRACTIVE INDEX OF BK7 GLASS MEASURED BY THZ-TDS

In order to test the experiment setup for THz-TDS, we have measured the complex refractive index of the commercial available BK7 glass from which the glass slides are made. The lateral size and thickness of the sample are 1.5

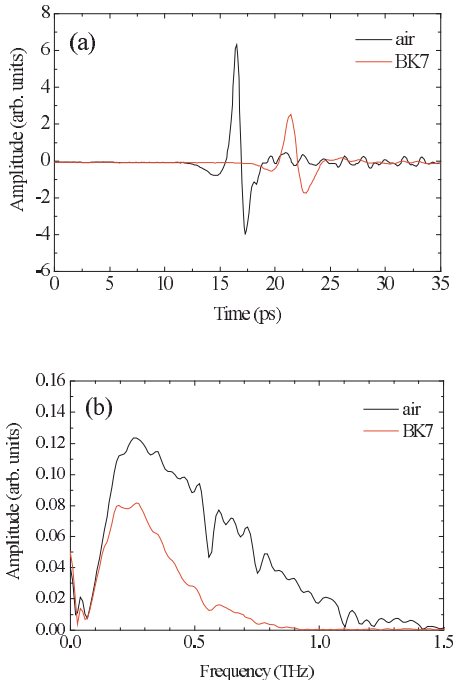

FIG. 2. (Color online) Waveform (a) and frequency spectrum (b) of the THz pulse transmitted through a 1 mm-thick BK7 glass. For comparison, the waveform and frequency spectrum of the reference pulse (i.e., the pulse transmitted through air) are also plotted.

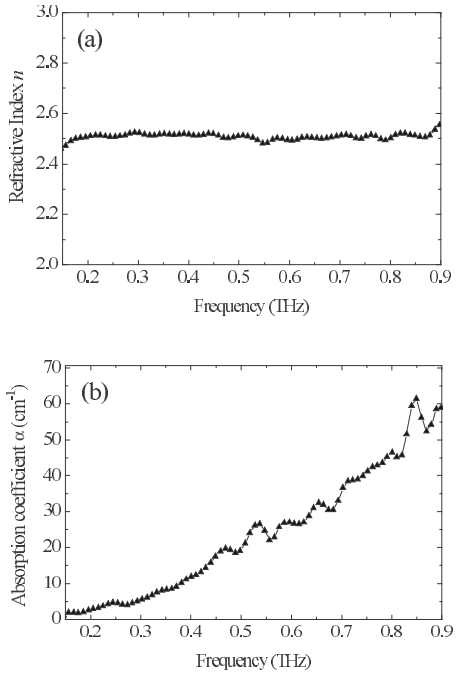

FIG. 3. (a) Refractive index and (b) absorption coefficient of the BK7 glass derived from THz-TDS by using Eqs. (1)–(4).

$\times 1.5$ cm^2 and 1 mm, respectively. In THz-TDS measurements, the time extent of the THz pulse scan was chosen to be 102.4 ps (i.e., 1024 measurement points with a time interval of 0.1 ps). However, it was found that for the BK7 glass the waveform of the pulse after 35 ps was influenced by the strong reflection from the backside of the sample. If we chose a time window of 35 ps for Fourier transformation, then the resolution of the frequency spectrum would be low. To perform a numerical interpolation between the measured frequency points, the measured pulse in time domain was extended with zero (zero padding) to 102.4 ps which is about three times the scan duration. This method has been used by many researchers to improve the resolution of the frequency spectra.[20,24,25] The amplitude and phase of the transmitted wave can be derived from the measured time-domain data of the electric field using a standard fast Fourier transformation. The transient electric field and transmission spectrum for BK7 glass are presented in Figs. 2(a) and 2(b), respectively. For comparison, the data of the reference sample (air) is also provided.

Basically, the refractive index $n(\omega)$ and absorption coefficient $\alpha(\omega)$ of a material can be easily derived by using the following formulas once the amplitude and phase of the transmission spectrum are known:[26]

$$A(\omega) = \frac{E_s(\omega)}{E_r(\omega)}, \tag{1}$$

$$\varphi(\omega) = \varphi_s(\omega) - \varphi_r(\omega), \tag{2}$$

$$n(\omega) = \frac{\varphi(\omega)c}{\omega d} + 1, \tag{3}$$

$$\alpha(\omega) = \frac{2}{d}\ln\left[\frac{4n(\omega)}{A(\omega)[n(\omega)+1]^2}\right]. \tag{4}$$

Here, ω is the angular frequency of the THz wave, $E_r(\omega)$ and $E_s(\omega)$ are the amplitudes of the electric field of the THz wave transmitted through air and the sample, $A(\omega)$ and $\varphi(\omega)$ are the normalized amplitude and phase shift in the transmitted wave, d is the thickness of the sample, and c is the speed of light in vacuum.

The optical properties of BK7 glass calculated by using Eqs. (1)–(4) are shown in Fig. 3. It is found that the refractive index of BK7 glass in the frequency range of 0.1–0.9 THz is nearly a constant ($n=2.5$). Meanwhile, the absorption coefficient exhibits a linear increase in this frequency range. However, its value is less than 30 cm^{-1} for frequencies lower than 0.5 THz. Our measurement results are similar to those reported previously by Naftaly *et al.*[27]

IV. CHARACTERIZATION OF 1D PCS WITHOUT AND WITH A DEFECT

In experiments, we first moved PC2 close to PC1. Then, we gradually increased the air gap between them and measured the transmitted THz signals from which the transmission spectra were derived. Different from the measurement of BK7 glass, no obvious refection from the backsides of the PC samples was observed and the time extent for pulse scans was chosen to be 102.4 ps. To clearly resolve the defect mode with a narrow linewidth, however, zero padding to 409.6 ps was also employed, corresponding to a frequency resolution of ~2.5 GHz in the frequency spectra. In Fig. 4(a), we show the evolution of the transmission spectrum with increasing size of the air gap (or the defect). When the air gap was set to be 50 μm, the periodicity of the PCs (PC1 and PC2) was maintained and the combination of the two

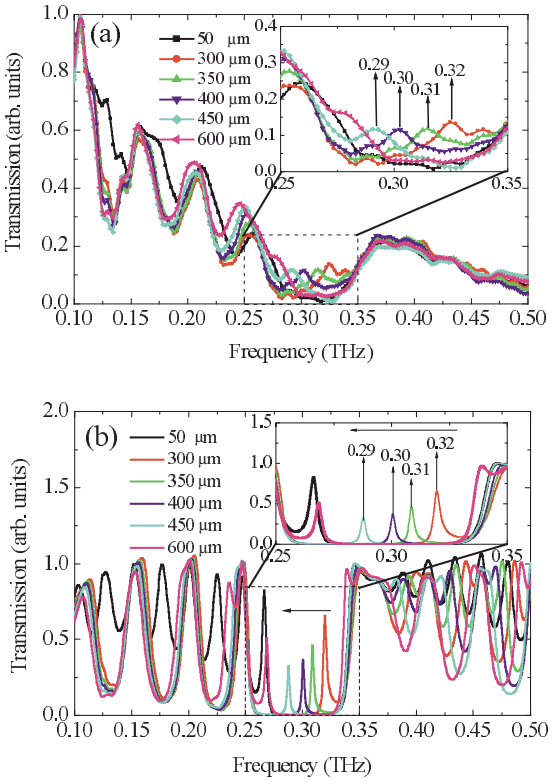

FIG. 4. (Color online) Experimental observation (a) and numerical simulation result (b) for the evolution of the transmission spectrum of the 1D PC with increasing size of the defect. $d=50$ μm corresponds to a perfect PC without a defect.

PCs formed a perfect PC with more periods. In this case, no defect mode was created. Even for larger defect sizes, no defect mode was observed in the PBGs. As the defect size was increased to 300 μm, however, a defect mode began to appear at 0.32 THz. It shifted to 0.31, 0.30, and 0.29 THz when the defect size was further increased to 350, 400, and 450 μm. When the defect size became 600 μm, the defect mode disappeared completely. In order to examine the validity of the experimental results, we have also performed numerical simulations for the same structures by using the finite-difference time-domain (FDTD) technique[28] and the results are presented in Fig. 4(b). The appearance and shift in the defect mode are in good agreement with those observed in the experiments. Since we did not include the absorption coefficient of the glass into the numerical simulations, the transmittance of both the pass bands and the defect mode appear to be higher in the simulation results.

V. MODIFYING THE DEFECT MODE OF THE 1D PC WITH A HIGH-RESISTIVITY SI WAFER: EXPERIMENT AND NUMERICAL SIMULATION

In order to investigate the modification of the defect mode, a 300 μm-thick silicon wafer with a high resistivity of 35 Ω cm was employed. In this case, the silicon wafer behaves as a dielectric material that is almost transparent to the THz wave. Its refractive index is measured to be about 3.4.[15] In experiments, the silicon wafer was gradually inserted into the air gap between PC1 and PC2 which was fixed to be 450 μm, as schematically shown in Fig. 5. The

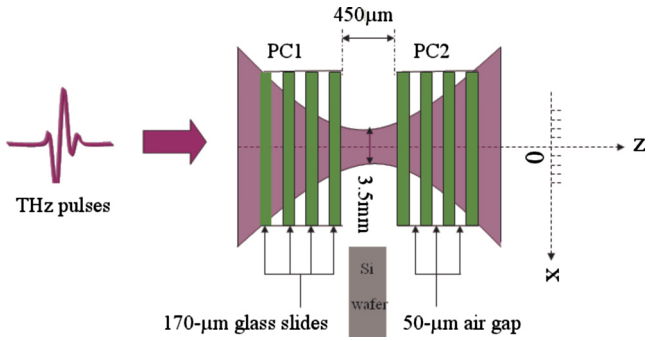

FIG. 5. (Color online) Schematic showing the modification of the defect mode of the 1D PC with the insertion of a silicon wafer.

waist of the THz beam where the sample was placed was estimated to be ~3.5 mm. At the initial stage, the front end of the silicon wafer was located at the edge of the diaphragm whose diameter was 4 mm. If we chose the coordinate shown in Fig. 5, then the front end of the silicon wafer was initially located at $x=2$ mm. Then, the silicon wafer was moved forward with a step of 1 mm. When $x=0$ mm, the front end of the silicon wafer was moved to the center of the THz beam. It implies that at least half of the beam experiences the phase change induced by the silicon wafer. As $x=-2$ mm, the whole beam was affected by the silicon wafer. The evolution of the transmission spectrum with the change in the silicon wafer position is shown in Fig. 6(a). It can be seen that the defect mode appeared at 0.29 THz when the silicon wafer was out of the THz beam ($x=2$ mm). In this case, the defect was formed by the 450 μm-thick air gap. When $x=1$ mm, the defect mode was perturbed by the silicon wafer. As a result, the transmittance was slightly attenuated. Meanwhile, a small peak began to appear at the higher frequency of 0.31

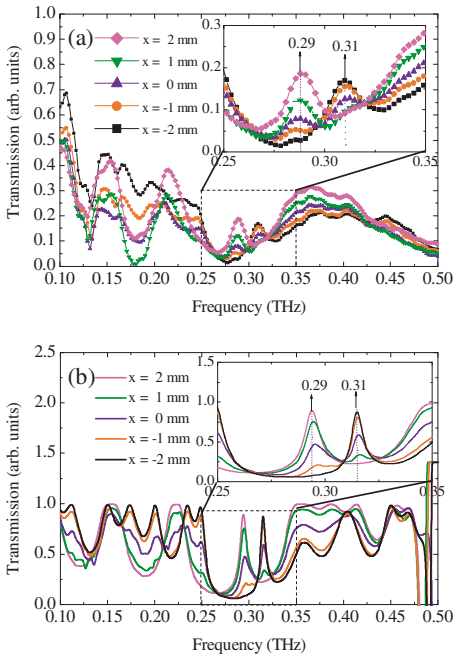

FIG. 6. (Color online) Experimental observation (a) and numerical simulation result (b) for the evolution of the transmission spectrum of the 1D PC with a defect with the change in the position of the inserted silicon wafer whose resistivity is 35 Ω cm.

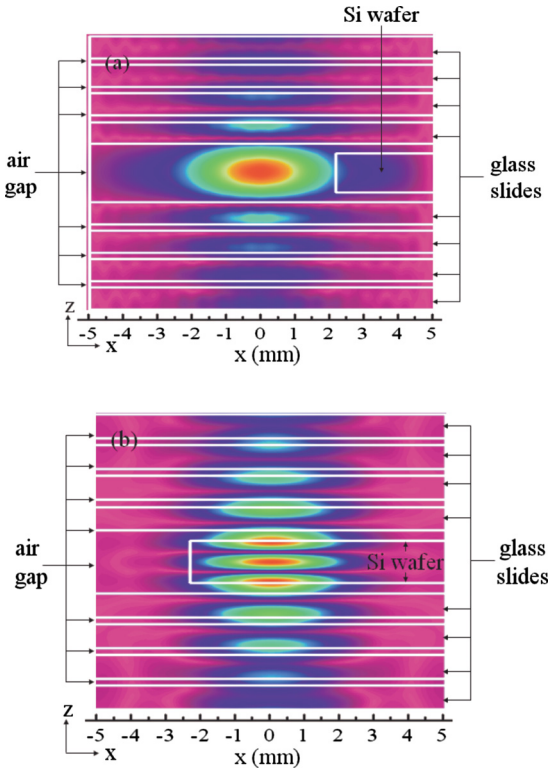

FIG. 7. (Color online) Electric field distribution in the defect before (a) and after (b) the complete insertion of the silicon wafer into the defect.

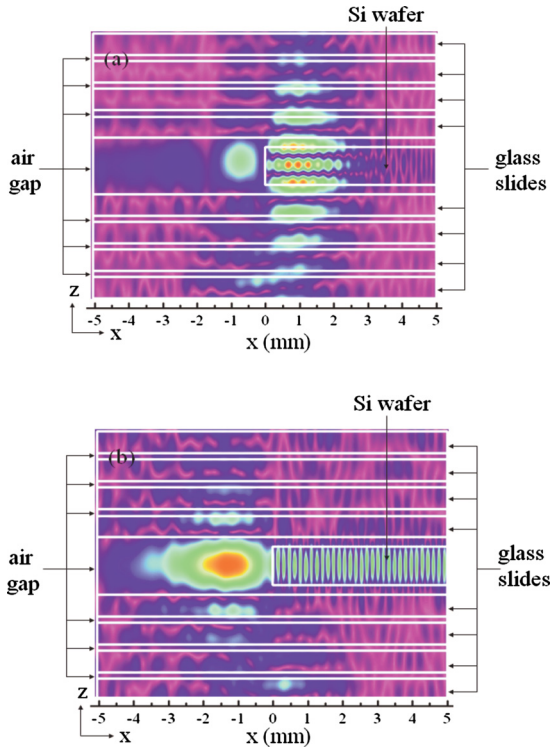

FIG. 8. (Color online) Electric field distributions of the defect modes at 0.31 THz (a) and 0.29 THz (b) when the front end of the silicon wafer was located at the center of the THz beam.

THz. As $x=0$ mm, the transmittance of the defect mode at 0.29 THz was further reduced while that of the new defect mode at 0.31 THz was enhanced. In this case, we can identify two defect modes clearly. For $x=-1$ mm, the defect mode at 0.29 THz almost disappeared and the defect mode at 0.31 THz became dominant. Finally, only the defect mode at 0.31 THz was observed when $x=-2$ mm. In this experiment, we clearly observed the transition of the defect mode from one frequency (0.29 THz) to the other (0.31 THz) after the insertion of the silicon wafer with a high resistivity. This transition can be attributed to the phase shift in the THz wave induced by the silicon wafer. With the appropriate choice of the wafer thickness (in our case 300 μm), the new defect mode appears in the PBG. An interesting phenomenon is the coexistence of the two defect modes which is observed at $x=0$ mm. The above experimental observations are confirmed by numerical simulation results shown in Fig. 6(b)

In order to gain a deep insight into the modification of the defect mode and especially the change in the distribution of the electric field, we also carried out numerical simulations for the modified PCs by using FDTD technique. A perfectly matched layer boundary condition was employed to ensure that the wave incident on the boundary is completely absorbed with negligible reflection. In addition, the lateral dimension of the simulation area was chosen to be 10 mm which is much larger than the diameter of the THz beam (3.5 mm). To do so, the THz beam was not squeezed between the boundaries in lateral dimension, similar to the situation in experiments. In Figs. 7(a) and 7(b), we show the distributions of the electric field in the defect for $x=2$ mm and -2 mm, respectively. It is apparent that the distribution of the electric field inside the defect is modified significantly after the complete insertion of the silicon wafer. We can identify two nodes in the field distribution for $x=-2$ mm. As mentioned above, two defect modes coexist when $x=0$ mm. The field distributions for the two defect modes are shown in Figs. 8(a) and 8(b). For the defect mode at 0.31 THz, the field distribution on the left side of the defect looks like the field distribution observed at $x=2$ mm while that on the right side assembles that observed at $x=-2$ mm. This phenomenon can be easily understood because $x=0$ mm behaves as the intermediate state between $x=2$ mm and $x=-2$ mm. More interestingly, the field distribution for the defect mode at 0.29 THz appears to be completely different. In this case, the transmission of the THz wave perpendicular to the glass slides is strongly attenuated. Instead, the propagation of the THz wave parallel to the glass slides, which is negligible in other cases, becomes significant. One can clearly see that the guide modes exist not only in the air gap on the left side but also in the silicon wafer on the right side. This behavior implies that the energy stored in the defect can be partially extracted by the silicon wafer. In other words, the propagation direction of the THz wave can be modified through the insertion of the silicon wafer with a high resistivity.

In order to further understand the coupling of the THz wave propagating in the z direction into the silicon wafer aligned in the x direction, we have placed three power monitors at different positions to detect the energy flow in the modified PC. One monitor (monitor 1) is placed just behind the PC to measure the transmitted power along the z direction while the other two are located on the right (monitor 2)

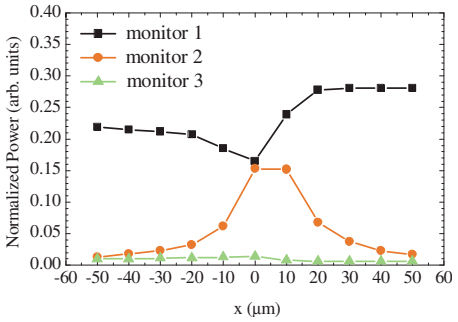

FIG. 9. (Color online) Dependence of the normalized powers detected by three monitors which are placed just behind the PC (monitor 1), and on the right (monitor 2) and left (monitor 3) sides of the defect. The coupling efficiency of the THz wave into the silicon wafer is indicated by monitor 2.

and left (monitor 3) sides of the defect to record the power coupled into the silicon wafer and that propagating in the air gap, respectively. A dependence of the detected power on the position of the front end of the silicon wafer for the three monitors is presented in Fig. 9. It can be seen that at $x=0$ mm nearly 15% of the incident power can be coupled into the silicon wafer. The coupling efficiency decreases rapidly when the front end of the silicon wafer is moved away from the beam center. For $x=50$ μm, no obvious coupling is observed. This phenomenon indicates that the energy stored in the defect can be only effective extracted out of the defect when the silicon wafer is located exactly at the center of the THz beam.

VI. MODIFYING THE DEFECT MODE OF THE 1D PC WITH A LOW-RESISTIVITY SI WAFER: EXPERIMENT AND NUMERICAL SIMULATION

In Sec. V, we have described the modification of the defect mode of the PC after inserting a silicon wafer with a high resistivity at different positions of the defect. In this case, the major effect of the silicon wafer is to induce a phase shift for the THz wave because the silicon wafer behaves as a dielectric material.

In this section, we will show how the defect mode is modified when a silicon wafer with a low resistivity is used. In this experiment, we chose a 200 μm-thick silicon wafer with a resistivity of 0.03 Ω cm. In this case, the silicon wafer behaves as a metal that is highly reflective for THz wave. The skin depth of the THz wave, which is estimated to be several hundred nanometers, is quite small as compared to the thickness of the silicon wafer. In order words, the THz wave cannot penetrate into the silicon wafer, leading to a negligible electric field inside the silicon wafer. We have performed similar experiments with the silicon wafer with a low resistivity and found only the attenuation of the transmittance of the defect mode is observed with the insertion of the silicon wafer. We did not see any new defect modes. This behavior is completely different from what we observed when the silicon wafer with a high resistivity was used. In Fig. 10, we show the field distributions of the electric field for $x=1$ and 0 mm obtained by FDTD simulations. In both cases, the electric field of the THz wave is prohibited in the silicon wafer. Consequently, the propagation path of the THz

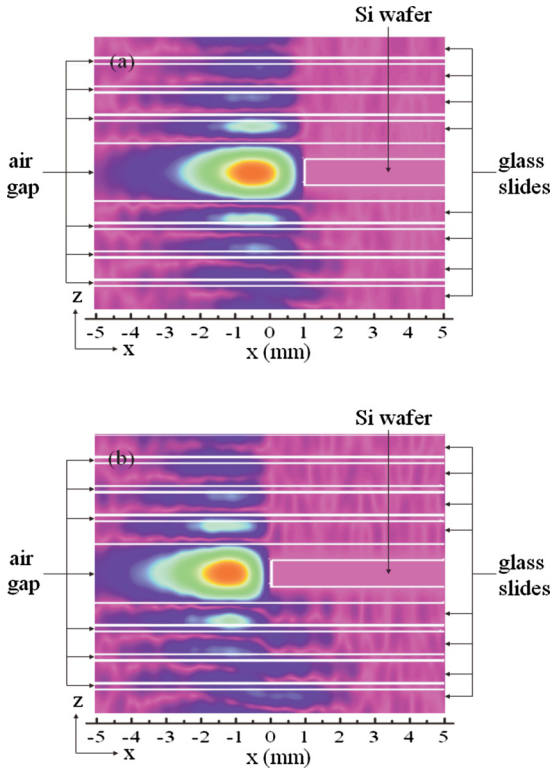

FIG. 10. (Color online) Electric field distributions of the defect modes when the front end of the silicon wafer was located at (a) $x=1$ mm and (b) $x=0$ mm.

wave is pushed to the left side when x is changed from 1 to 0 mm. This is responsible for the reduction in the transmittance of the defect mode. Since there is no apparent change in the field distribution, no new defect mode is created.

VII. CONCLUSION

In summary, we have constructed 1D PCs in THz spectral region by using glass slides and systematically investigated the modification of the defect mode in the PCs by employing THz-TDS. It is found that the defect mode in such a PC can be easily modified by inserting a silicon wafer into the defect region. Both the transmittance and the resonant frequency of the defect mode can be modified and the modification depends strongly on the resistivity of the inserted silicon wafer. When a high-resistivity silicon wafer was used, a transition of the defect mode from one frequency to the other was observed after the insertion of the silicon wafer. More interestingly, two defect modes coexist when the silicon wafer was located at the center of the THz beam. In this case, the energy stored in the defect can be partially extracted by the silicon wafer. For the silicon wafer with a low resistivity, we observed only the attenuation of the defect mode. The field distribution inside the defect was pushed to the left side by the silicon wafer that behaves as a metal. Our research results indicate that PCs in THz spectral region may offer us the opportunity for investigating and understanding the physical mechanism responsible for the modification of defect modes. Some interesting behaviors may find applications in controlling the propagation of THz wave.

ACKNOWLEDGMENTS

The authors acknowledge the financial support from the National Natural Science Foundation of China (Grant Nos. 10974060 and 10774050) and the Program for Innovative Research Team of the Higher Education in Guangdong province of China (Grant No. 06CXTD005).

[1]J. D. Joannopoulos, R. D. Meade, and J. N. Winn, *Photonic Crystals: Molding the Flow of Light* (Princeton University Press, Princeton, N. J., 1995).
[2]K. Inoue and K. Ohtaka, *Photonic Crystals: Physics, Fabrication, and Applications* (Springer-Verlag, Berlin, 2004).
[3]J. S. Foresi, P. R. Villeneuve, J. Ferrera, E. R. Thoen, G. Steinmeyer, S. Fan, J. D. Joannopoulos, L. C. Kimerling, H. I. Smith, and E. P. Ippen, Nature (London) **390**, 143 (1997).
[4]A. Yariv, Y. Xu, R. K. Lee, and A. Scherer, Opt. Lett. **24**, 711 (1999).
[5]M. Bayer, T. Gutbrod, A. Forchel, T. L. Reinecke, P. A. Knipp, R. Werner, and J. P. Reithmaier, Phys. Rev. Lett. **83**, 5374 (1999).
[6]S. Lan, S. Nishikawa, H. Ishikawa, and O. Wada, J. Appl. Phys. **90**, 4321 (2001).
[7]P. R. Villeneuve, D. S. Abrams, S. Fan, and J. D. Joannopoulos, Opt. Lett. **21**, 2017 (1996).
[8]S. Lan, A. V. Gopal, K. Kanamoto, and H. Ishikawa, Appl. Phys. Lett. **84**, 5124 (2004).
[9]X. Y. Hu, Q. H. Gong, Y. H. Liu, B. Y. Cheng, and D. Z. Zhang, Appl. Phys. Lett. **87**, 231111 (2005).
[10]X. Y. Hu, P. Jing, C. Y. Ding, H. Yang, and Q. H. Gong, Nat. Photonics **2**, 185 (2008).
[11]H. Y. Liu, S. Lan, L. J. Wu, Q. Guo, W. Hu, S. H. Liu, X. S. Lin, and A. V. Gopal, Appl. Phys. Lett. **90**, 213507 (2007).
[12]D. Englund, A. Faraon, I. Fushman, N. Stoltz, P. Petroff, and J. Vučković, Nature (London) **450**, 857 (2007).
[13]I. Märki, M. Salt, and H. P. Herzig, Opt. Express **14**, 2969 (2006).
[14]H. Němec, P. Kužel, F. Garet, and L. Duvillaret, Appl. Opt. **43**, 1965 (2004).
[15]P. Mounaix, E. Freysz, J. Degert, N. Daro, J.-F. Létard, P. Kužel, V. Vigneras, and L. Oyenhart, Appl. Phys. Lett. **89**, 174105 (2006).
[16]B. Ferguson and X. C. Zhang, Nature Mater. **1**, 26 (2002).
[17]K. Sakai, *Terahertz Optoelectronics* (Springer-Verlag, Berlin, 2005).
[18]M. Tonouchi, Nat. Photonics **1**, 97 (2007).
[19]P. Mukherjee and B. Gupta, Int. J. Infrared Millim. Waves **29**, 1091 (2008).
[20]D. X. Qu, D. Grischkowsky, and W. L. Zhang, Opt. Lett. **29**, 896 (2004).
[21]W. L. Zhang, A. K. Azad, J. G. Han, J. Z. Xu, J. Chen, and X. C. Zhang, Phys. Rev. Lett. **98**, 183901 (2007).
[22]M. C. Wanke, O. Lehmann, K. Müller, Q. Wen, and M. Stuke, Science **275**, 1284 (1997).
[23]Z. P. Jian, J. Pearce, and D. M. Mittleman, Opt. Lett. **29**, 2067 (2004).
[24]H. B. Liu and X. C. Zhang, in *Terahertz Frequency Detection and Identification of Materials and Objects* (Springer, Berlin, 2007).
[25]S. S. Harsha, N. Laman, and D. Grischkowsky, Appl. Phys. Lett. **94**, 091118 (2009).
[26]S. L. Dexheimer, *Terahertz Spectroscopy: Principles and Applications* (CRC, Boca Raton, FL, 2008).
[27]M. Naftaly and R. E. Miles, in *Terahertz Frequency Detection and Identification of Materials and Objects* (Springer, Berlin, 2007).
[28]In this paper, a commercially available software developed by Rsoft Design Group (http://www.rsoftdesign.com) is used for the numerical simulations.